Title	Perpendicularly magnetized Mn60Ga40 films on Ge(001) grown at low temperature
Author(s)	Nishioka, M.; Kakutani, T.; Kiire, T. et al.
Citation	Journal of Magnetism and Magnetic Materials. 2025, 630, p. 173338
Version Type	VoR
URL	https://hdl.handle.net/11094/102775
rights	This article is licensed under a Creative Commons Attribution 4.0 International License.
Note	

Journal of Magnetism and Magnetic Materials 630 (2025) 173338

Contents lists available at ScienceDirect

Journal of Magnetism and Magnetic Materials

journal homepage: www.elsevier.com/locate/jmmm

Research article

Perpendicularly magnetized $Mn_{60}Ga_{40}$ films on Ge(001) grown at low temperature

M. Nishioka [a], T. Kakutani [a], T. Kiire [a], T. Usami [b,c,*], S. Yamada [a,b,c], K. Hamaya [a,b,c]

[a] Department of Systems Innovation, Graduate School of Engineering Science, The University of Osaka, Toyonaka, 560-8531, Osaka, Japan
[b] Center for Spintronics Research Network, Graduate School of Engineering Science, The University of Osaka, Toyonaka, 560-8531, Osaka, Japan
[c] Spintronics Research Network Division, Institute for Open and Transdisciplinary Research Initiatives, The University of Osaka, Suita, 565-0871, Osaka, Japan

A R T I C L E I N F O

Keywords:
$L1_0$-$Mn_{60}Ga_{40}$
Semiconductor
Spintronic device
Crystal growth

A B S T R A C T

Perpendicularly magnetized materials hold significant potential for high density integration of nonvolatile spintronic memories and semiconductor spintronic devices. Here we show a perpendicularly magnetized $Mn_{60}Ga_{40}$ film grown on a semiconductor Ge at 100°C. Using a low-temperature molecular beam epitaxy technique, we finely control the composition of thin Co_xFe_{100-x} buffer layers for the growth of $L1_0$-$Mn_{60}Ga_{40}$. We find that an $L1_0$-$Mn_{60}Ga_{40}$ film with a $Co_{67}Fe_{33}$/Fe bilayer buffer structure shows perpendicular magnetic properties even on Ge. This study paves the way for perpendicular magnetic tunnel junctions with a low resistance-area product or semiconductor spintronic devices with perpendicularly magnetized spin injector/detector electrodes.

1. Introduction

Developing spintronics devices, such as a magnetoresistive random-access memory (MRAM) [1–4], a spin metal–oxide–semiconductor field-effect transistor (spin-MOSFET) [5], and a spin-polarized light-emitting diodes (spin-LED) [6], has been explored in the field of next-generation low-power consumption electronic devices. It is well known that these devices have ferromagnetic electrodes for nonvolatile memory effect with large resistance changes via magnetoresistance effect. For highly integrated devices and systems, the ferromagnetic electrodes should be perpendicularly magnetized materials including improved thermal stability and miniaturization potential [7–9]. Several materials and structures have already been explored to achieve perpendicularly magnetized electrodes, such as Co/Pd multilayers and CoFeB/MgO utilizing interfacial perpendicular magnetic anisotropy (PMA) [7,10,11]. Unfortunately, the use of MgO-based structures suffers from high parasitic resistance, increasing power consumption in spintronic devices [12]. If intrinsic perpendicularly magnetized electrodes were realized in such spintronics devices, one could open a way for highly integrated devices and systems without using MgO for the interfacial PMA.

One of the promising materials is a Mn-Ga alloy. An $L1_0$-ordered Mn-Ga structure exhibits strong PMA and excellent thermal stability [13–18], making it an ideal candidate for magnetic tunnel junctions (MTJs) in MRAM. On the other hand, for semiconductor spintronic devices such as spin-MOSFET and spin-LED, there are few reports on the fabrication of perpendicularly magnetized Mn-Ga. In particular, whereas $L1_0$-ordered Mn-Ga films have been successfully grown on GaAs [19,20], limited reports exist on its growth on Si [21] and Ge, which are potential candidate semiconductors for room-temperature semiconductor spintronic devices [22–25].

To achieve $L1_0$-ordered Mn-Ga even on Si and Ge, we should consider the next requirements. First, for high-performance heterointerface, a low-temperature growth method for $L1_0$-ordered Mn-Ga should be used. However, anneal processes at temperatures ranging from 250°C to 500°C have generally been utilized in most previous studies [26–28]. Next, because the epitaxial growth of $L1_0$-ordered Mn-Ga directly on Si or Ge is challenging, the use of a ferromagnetic buffer layer should be examined [29]. In this regard, since there are successful examples of low-temperature growth on non-magnetic CoGa [15], we can change the non-magnetic CoGa to a ferromagnetic material with a lattice constant similar to that of CoGa.

In this study, we explore epitaxial growth of $L1_0$-ordered $Mn_{60}Ga_{40}$ on Ge(001) with a Co_xFe_{100-x} buffer layer, as shown in Fig. 1(a), as a candidate structure for room-temperature semiconductor spintronic devices. Using a low-temperature (100°C) molecular beam epitaxy (MBE) technique, we finely control the composition of Co_xFe_{100-x} buffer layers on top of Ge(001). When we use a 1-nm-thick $Co_{67}Fe_{33}$/1-nm-thick Fe bilayer buffer structure, an $L1_0$-$Mn_{60}Ga_{40}$ layer with perpendicular magnetization is epitaxially grown on Ge(001). This study paves the

* Corresponding author at: Center for Spintronics Research Network, Graduate School of Engineering Science, The University of Osaka, Toyonaka, 560-8531, Osaka, Japan.

E-mail addresses: usami.takamasa.es@osaka-u.ac.jp (T. Usami), hamaya.kohei.es@osaka-u.ac.jp (K. Hamaya).

https://doi.org/10.1016/j.jmmm.2025.173338
Received 29 April 2025; Received in revised form 10 June 2025; Accepted 30 June 2025
Available online 10 July 2025

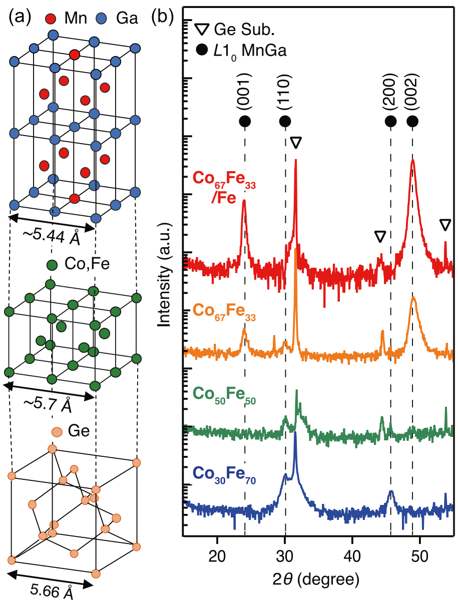

Fig. 1. (a) A schematic of the target epitaxial relationships among $Mn_{60}Ga_{40}$, Co_xFe_{100-x} buffer layer, and Ge(001) substrate. (b) ω-2θ XRD patterns of the $Mn_{60}Ga_{40}/Co_xFe_{100-x}$ with x = 30, 50, 67 and $Mn_{60}Ga_{40}/Co_{67}Fe_{33}/Fe$ structure.

way for highly integrated semiconductor spintronic devices and systems without using MgO for the interfacial PMA.

2. Experimental method

Fig. 1(a) shows a schematic of the target stacking structures in this study. The detailed layer configurations are as follows (thickness in nm): Si(2)/$Mn_{60}Ga_{40}$(30)/Co_xFe_{100-x}(2)/Ge(001) substrate and Si(2)/$Mn_{60}Ga_{40}$(30)/$Co_{67}Fe_{33}$(1)/Fe(1)/Ge(001) substrate. Here, we intentionally choose $Mn_{60}Ga_{40}$ composition due to its strong PMA [30] and to high magnetoresistance in MTJ structures with MnGa as the bottom electrode and MgO as the tunnel barrier [31]. As shown in Fig. 1(a), the epitaxial growth relationship among $Mn_{60}Ga_{40}$, Co_xFe_{100-x} buffer layer, and Ge(001) substrate are expected to be very good. In particular, $Mn_{60}Ga_{40}$ requires c-axis orientation to exhibit PMA, making its precise epitaxial alignment critical for achieving high-performance perpendicular magnetic tunnel junctions.

The samples were grown using an MBE system under an ultra-high vacuum of 10^{-7} Pa. Prior to loading the commercial Ge(001) substrate ($\rho \sim 5$ Ωcm) into an MBE chamber, we performed surface cleaning of the substrate with an aqueous 1% HF solution to remove native oxide and contamination. The loaded substrate was heated at 450°C for 20 min in the MBE chamber, followed by cooling down to the growth temperature of 100°C. Co_xFe_{100-x} and $Mn_{60}Ga_{40}$ layers were grown via co-deposition of Co and Fe, and Mn and Ga, respectively, using Knudsen cells. The deposition rates were measured using a beam flux monitor equipped with a Bayard-Alpert (B-A) gauge, and the deposition rates of Co, Fe, Mn, and Ga were calibrated by measuring the thickness of each film with a stylus profilometer. The Co composition, x, was varied to 66, 50, and 30 based on preliminary optimization of the Co_xFe_{100-x} buffer layer growth. The composition of the Mn-Ga films was determined by energy-dispersive X-ray (EDX) elemental mapping, while that of the Co-Fe films was estimated based on the growth rates, as the Co-Fe films were too thin for accurate determination by EDX mapping. Structural characterization of the grown films was performed using X-ray diffraction (XRD) and high-angle annular dark-field scanning transmission electron microscopy (HAADF-STEM). No filtering was applied to the HAADF-STEM images. Magnetization curves were measured at 300 K using a vibrating sample magnetometer under magnetic fields applied in both the out-of-plane and in-plane directions.

3. Results and discussion

Fig. 1(b) shows ω–2θ XRD patterns for the $Mn_{60}Ga_{40}$(30)/Co_xFe_{100-x}(2) with x = 30, 50, 67 and $Mn_{60}Ga_{40}$(30)/$Co_{67}Fe_{33}$(1)/Fe(1) structure (thickness in nm). For the $Mn_{60}Ga_{40}/Co_{67}Fe_{33}$/Fe structure, we describe the detail explanation in the next paragraph. Focusing on the data for the $Co_{67}Fe_{33}$ (x = 67) buffer layer without an Fe insertion layer, we find distinct (001) and (002) peaks deriving from $L1_0$-$Mn_{60}Ga_{40}$, indicating that the (001)-oriented $L1_0$-$Mn_{60}Ga_{40}$ layer has PMA on Ge(001). However, as the Co composition decreases ($x \leq 50$), other peaks deriving from $L1_0$-$Mn_{60}Ga_{40}$ (110) and (200) are observed, which can imply a deterioration in PMA. These trends can be explained by the increase in the lattice mismatch between Co_xFe_{100-x} and $L1_0$-$Mn_{60}Ga_{40}$ as follows. When the Co composition is relatively small ($x < 20$), the lattice mismatch exceeds 5.2%, too large to grow (001)-oriented $L1_0$-$Mn_{60}Ga_{40}$. As the Co content increases, on the other hand, the mismatch gradually decreases, reaching approximately 4.4% at x = 67. We infer that the reduction in the lattice mismatch enables the possibility of the growth of (001)-oriented $L1_0$-$Mn_{60}Ga_{40}$ on top of Co_xFe_{100-x}. If the Co composition is further increased ($x \geq 67$), the structural transition from the bcc phase to the face-centered cubic (fcc) one occurs in the Co_xFe_{100-x}. In this case, the epitaxial growth of the Co_xFe_{100-x} on Ge(001) is expected to be difficult. Therefore, for achieving the (001)-oriented $L1_0$-$Mn_{60}Ga_{40}$, we should finely control x to achieve the optimum Co_xFe_{100-x} buffer layer.

Here, it is known that atomic interdiffusion between Co and Ge easily occurs at the Co-based alloy/Ge heterointerface [32,33]. Thus, we should deeply consider the atomic interdiffusion between Co and Ge in the $Mn_{60}Ga_{40}/Co_{67}Fe_{33}$/Ge(001) structure. In this study, we adapt the use of an Fe insertion layer to suppress the atomic interdiffusion between Co and Ge [12,34]. That is, we utilize a $Co_{67}Fe_{33}$/Fe bilayer structure as a buffer layer for $L1_0$-$Mn_{60}Ga_{40}$ on Ge(001). As shown in the red curve in the XRD pattern in Fig. 1(b), we evidently obtain larger intensity from the (001) and (002) peaks derived from $L1_0$-$Mn_{60}Ga_{40}$ for the $Co_{67}Fe_{33}$/Fe bilayer buffer than those for the $Co_{67}Fe_{33}$ single layer one. We speculate that the use of the Fe insertion layer enables us to grow highly (001)-oriented $L1_0$-$Mn_{60}Ga_{40}$ layer on Ge(001) because of the suppression of the atomic interdiffusion between Co and Ge near the heterointerface.

To confirm its microscopic structures, we evaluate the stacked structure using HAADF-STEM and EDX measurements. Fig. 2(a) and (b) show low-magnification HAADF-STEM image for the $L1_0$-$Mn_{60}Ga_{40}/Co_{67}Fe_{33}$/Fe on Ge(001) and its EDX elemental mapping images, respectively. Although there are some roughnesses on top of the Ge substrate, we find the layered stacked structure consisting of Fe and Co elements. Notably, we cannot clearly distinguish between the $Co_{67}Fe_{33}$ and Fe layers because of the presence of Fe in both layers. On the $Co_{67}Fe_{33}$/Fe layer, a homogeneous layer consisting of Mn and Ga is observed, indicating the $Mn_{60}Ga_{40}$ layer. From these elemental mappings, we can judge that the atomic interdiffusion between Co and Ge is relatively suppressed during the growth, as mentioned in previous paragraph. Thus, in addition to the low-temperature growth at 100°C, the use of the $Co_{67}Fe_{33}$/Fe bilayer buffer structure is quite important in this study.

Fig. 2(c)–(e) display the high-resolution HAADF-STEM images for the enclosed regions near the interface between the grown layers and Ge substrate. We evidently see the lattice images with and without forming atomically ordered arrangements in Fig. 2(d). Namely, atomically ordered $Mn_{60}Ga_{40}$ layers are clearly formed on top of the random atomic Co-Fe alloy one, as designed in the growth recipe. Here, it is also found that the Mn-Ga region shows tetragonal $L1_0$ structure while the Co-Fe one is square corresponding to the bcc structure (see illustrations). It is surprising that the $L1_0$-ordered layer is achieved directly above the buffer layer even at 100°C. Concentrating on Fig. 2(e), we also find certain regions with atomic arrangement disorder like dislocation as shown in the illustrations. We infer that there are due to

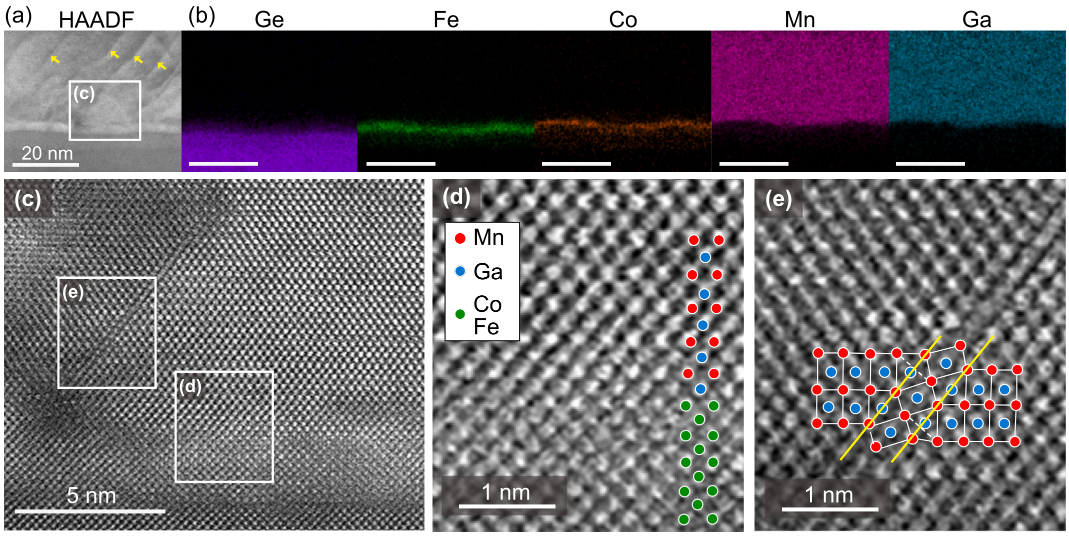

Fig. 2. (a) Low-magnification HAADF-STEM and (b) EDX elemental mapping images for the $Mn_{60}Ga_{40}/Co_{67}Fe_{33}$/Fe/Ge structure. The yellow arrows indicate atomic arrangement disorders such as dislocations. (c)–(e) High-resolution HAADF-STEM images for the enclosed regions. Tetragonal and cubic structures consisting of Mn-Ga and Co-Fe, respectively, are illustrated in (d) and (e).

the approximately 4.4% lattice mismatch between $L1_0$-$Mn_{60}Ga_{40}$ and $Co_{67}Fe_{33}$, as discussed in Fig. 1. These atomic arrangement disorder originates from the patterns showing yellow arrows in Fig. 2(a). It is interesting that the disorder like dislocation is formed within a half unit cell of $L1_0$-$Mn_{60}Ga_{40}$ and (001)-oriented structure is maintained over the observed regions. Unfortunately, since the surface flatness of the commercial Ge substrate is relatively poor as shown in the low magnification images, we expect that the influence of the surface quality on the growth is able to be improved in future.

Finally, we evaluate PMA for the low-temperature grown $L1_0$-$Mn_{60}Ga_{40}$ film on Ge(001). Fig. 3(a) shows magnetization hysteresis (M-H) curves under sweeping out-of-plane (red) and in-plane (blue) magnetic fields (H) at 300 K for an $Mn_{60}Ga_{40}/Co_{67}Fe_{33}$/Fe/Ge structure. Since an easy-axis like hysteresis loop is observed by applying out-of-plane H, we understand that clear PMA arising from (001)-oriented $L1_0$-$Mn_{60}Ga_{40}$ is demonstrated. From the comparison of the data between red and blue curves, magnetocrystalline anisotropy constant (K_u) is roughly estimated to be 0.42 MJ/m^3. This value is approximately one-sixth of the theoretical value of 2.6 MJ/m^3 [35] and lower than previous experimental studies (1~2 MJ/m^3) [26–28]. As discussed in previous figures, *e.x.*, Fig. 2(e), the small value of K_u is due to the formation of the atomic arrangement disorder like dislocation, including non-(001)-oriented $L1_0$-$Mn_{60}Ga_{40}$. As a result, the reduction of (001)-oriented $L1_0$-$Mn_{60}Ga_{40}$ results in the dispersion of PMA in the film plane. We should further explore optimum growth conditions for obtaining fully (001)-oriented $L1_0$-$Mn_{60}Ga_{40}$ without forming atomic arrangement disorder. In addition, since the in-plane anisotropy of the CoFe/Fe layer can weaken the PMA induced by the MnGa layer, realizing a much thinner ferromagnetic layer can also lead to an improvement in PMA. When M-H curves for an $Mn_{60}Ga_{40}/Co_{67}Fe_{33}$/Ge structure (without the Fe interlayer) are measured, further small PMA can be observed as shown in Fig. 3(b). This also means that forming highly (001)-oriented $L1_0$-$Mn_{60}Ga_{40}$ is quite important for obtaining the strong PMA. As shown in the inset for the $Mn_{60}Ga_{40}/Co_{30}Fe_{70}$/Ge structure, if M-H curves for $Mn_{60}Ga_{40}$ films without forming the (001)-oriented $L1_0$ structure were measured, only in-plane magnetic anisotropy could be obtained. For the $Mn_{60}Ga_{40}/Co_{50}Fe_{50}$/Ge structure, a deterioration of PMA was also observed (data not shown). From these evaluations, we conclude that the formation of (001)-oriented $L1_0$-$Mn_{60}Ga_{40}$ layers is strongly related to PMA on Ge(001). In this study, even for the low-temperature growth on Ge(001), (001)-oriented $L1_0$-$Mn_{60}Ga_{40}$ having PMA is demonstrated by using MBE techniques

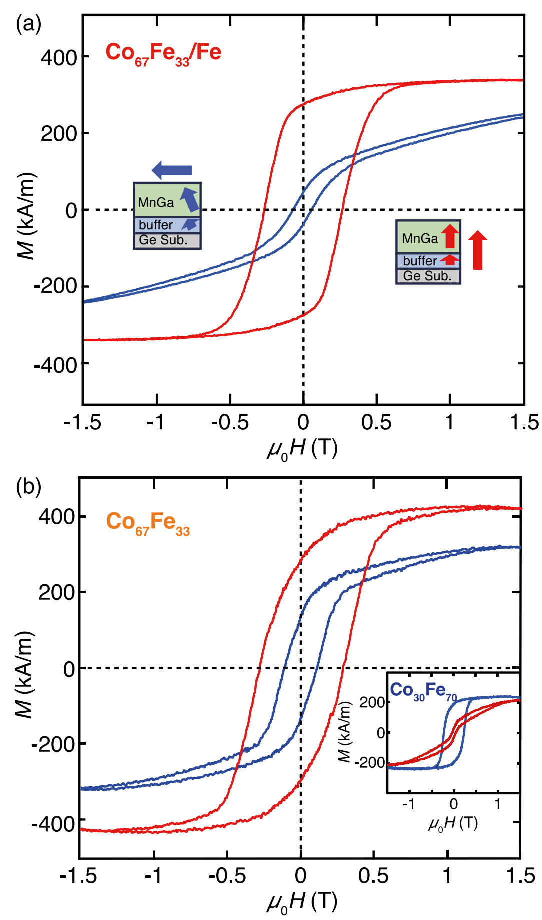

Fig. 3. M-H curves at 300 K for (a) $Mn_{60}Ga_{40}/Co_{67}Fe_{33}$/Fe and (b) $Mn_{60}Ga_{40}/Co_{67}Fe_{33}$ films grown on Ge(001). Red and blue curves are results measured under out-of-plane and in-plane H, respectively. The inset in (a) illustrates magnetization vectors of the stacked structure in measurements. The inset in (b) shows M-H curves at 300 K for an $Mn_{60}Ga_{40}/Co_{30}Fe_{70}$ film on Ge(001).

and an optimum buffer layer structure. Finally, we briefly comment on the interfacial exchange coupling at the MnGa/Co_xFe_{100-x} interface. A previous study reported that the interfacial exchange coupling in the Co_xFe_{100-x}/MnGa structure depends on the Co_xFe_{100-x} composition and influences the magnetic-field dependence of the magnetoresistance [36]. Although it is not yet clear whether the interfacial exchange coupling in the present $Mn_{60}Ga_{40}/Co_{67}Fe_{33}$ system is ferromagnetic or antiferromagnetic, magnetoresistance measurements using magnetic tunnel junctions can provide direct evidence. This will be an important subject for future investigation.

4. Conclusions

In conclusion, we have explored a perpendicularly magnetized $Mn_{60}Ga_{40}$ film grown on a semiconductor Ge at 100°C. By adjusting the composition of Co_xFe_{100-x} buffer layer to $x = 67$ and inserting a 1-nm-thick Fe layer on Ge, an $L1_0$-$Mn_{60}Ga_{40}$ film with PMA was demonstrated even on Ge. This study paves the way for perpendicular magnetic tunnel junctions with a low resistance-area product or semiconductor spintronic devices with perpendicular magnetized spin injector/detector electrodes.

CRediT authorship contribution statement

M. Nishioka: Investigation, Writing – original draft, Writing – review & editing. **T. Kakutani:** Investigation. **T. Kiire:** Investigation. **T. Usami:** Writing – review & editing. **S. Yamada:** Writing – review & editing. **K. Hamaya:** Funding acquisition, Supervision, Writing – review & editing.

Declaration of competing interest

The authors declare that they have no known competing financial interests or personal relationships that could have appeared to influence the work reported in this paper.

Acknowledgments

The authors acknowledge Prof. Y. Niimi, Prof. Y. Suzuki, and Prof. Y. Nakamura of The University of Osaka for lots of experimental supports. This work was supported by JSPS KAKENHI (Grant Nos. 21H05000, 22H04964, 24H00034), MEXT X-NICS (Grant No. JPJ011438), and the Spintronics Research Network of Japan (Spin-RNJ).

Data availability

Data will be made available on request.

References

[1] A.D. Kent, D.C. Worledge, A new spin on magnetic memories, Nat. Nanotechnol 10 (2015) 187.
[2] S. Bhatti, R. Sbiaa, A. Hirohata, H. Ohno, S. Fukami, S. Piramanayagam, Spintronics based random access memory: a review, Mater. Today 20 (2017) 20.
[3] S. Yuasa, D.D. Djayaprawira, Giant tunnel magnetoresistance in magnetic tunnel junctions with a crystalline MgO(001) barrier, J. Phys. D: Appl. Phys. 40 (2007) R337.
[4] S. Ikegawa, F.B. Mancoff, J. Janesky, S. Aggarwal, Magnetoresistive random access memory: present and future, IEEE Trans. Electron Devices 67 (4) (2020) 1407.
[5] S. Sugahara, M. Tanaka, A spin metal–oxide–semiconductor field-effect transistor (spin MOSFET) with a ferromagnetic semiconductor for the channel, Appl. Phys. Lett. 84 (2004) 2307.
[6] M. Holub, P. Bhattacharya, Spin-polarized light-emitting diodes and lasers, J. Phys. D: Appl. Phys. 40 (2007) R179.
[7] S. Ikeda, K. Miura, H. Yamamoto, K. Mizunuma, H.D. Gan, M. Endo, S. Kanai, J. Hayakawa, F. Matsukura, H. Ohno, A perpendicular-anisotropy CoFeB-MgO magnetic tunnel junction, Nat. Mater. 9 (2010) 721–724.
[8] S. Yuasa, K. Hono, G. Hu, D.C. Worledge, Materials for spin-transfer-torque magnetoresistive random-access memory, MRS Bull. 43 (352) 5.
[9] B. Jinnai, K. Watanabe, S. Fukami, H. Ohno, Scaling magnetic tunnel junction down to single-digit nanometers - Challenges and prospects, Appl. Phys. Lett. 116 (2020) 160501.
[10] N. Perrissina nd S. Lequeux, N. Strelkov, A. Chavent, L. Vila, L.D. BudaPrejbeanu, S. Auffret, R.C. Sousa, I.L. Prejbeanu, B. Dieny, A highly thermally stable sub-20 nm magnetic random-access memory based on perpendicular shape anisotropy, Nanoscale 10 (2018) 12187.
[11] O. Golonzka, J.-G. Alzate, U. Arslan, M. Bohr, P. Bai, J. Brockman, B. Buford, C. Connor, N. Das, B. Doyle, T. Ghani, F. Hamzaoglu, P. Heil, P. Hentges, R. Jahan, D. Kencke, B. Lin, M. Lu, M. Mainuddin, M. Meterelliyoz, P. Nguyen, D. Nikonov, K. O'brien, J. ODonnell, K. Oguz, D. Ouellette, J. Park, J. Pellegren, C. Puls, P. Quintero, T. Rahman, A. Romang, M. Sekhar, A. Selarka, M. Seth, A.J. Smith, A.K. Smith, L. Wei, C. Wiegand, Z. Zhang, K. Fischeret, MRAM as embedded non-volatile memory solution for 22FFL FinFET technology, IEDM Tech. Dig. (2018) 18.1.1-18.1.4.
[12] M. Yamada, F. Kuroda, M. Tsukahara, S. Yamada, T. Fukushima, K. Sawano, T. Oguchi, K. Hamaya, Spin injection through energy-band symmetry matching with high spin polarization in atomically controlled ferromagnet/ferromagnet/semiconductor structures, NPG Asia Mater. 12 (2020) 47.
[13] T. Kubota, Y. Miura, D. Watanabe, S. Mizukami, F. Wu, H. Naganuma, X. Zhang, M. Oogane, M. Shirai, Y. Ando, T. Miyazaki, Magnetoresistance effect in tunnel junctions with perpendicularly magnetized $D0_{22}$-$Mn_{3-\delta}$Ga electrode and MgO barrier, Appl. Phys. Express 4 (2011) 043002.
[14] S.W. Mao, J. Lu, P. Zhao, X.L. Wang, D.H. Wei, J. Liu, J.B. Xia, J.H. Zhao, MnGa-based fully perpendicular magnetic tunnel junctions with ultrathin Co_2MnSi interlayers, Sci. Rep. 7 (2017) 43064.
[15] K. Kunimatsu, K.Z. Suzuki, S. Mizukami, Pseudomorphic deposition of $L1_0$-MnGa nanolayers at room temperature, J. Cryst. Growth 514 (2019) 8.
[16] K.Z. Suzuki, T. Ichinose, S. Iihama, R. Monma, S. Mizukami, Enhanced tunnel magnetoresistance in Mn-based perpendicular magnetic tunnel junctions utilizing antiferromagnetically coupled bcc-Co-based interlayer, Appl. Phys. Lett. 118 (2021) 172412.
[17] K.Z. Suzuki, S. Mizukami, Tunnel magnetoresistance exceeding 100% in magnetic tunnel junctions using Mn-based tetragonal alloy electrodes with perpendicular magnetic anisotropy, AIP Adv. 13 (2023) 035225.
[18] M. Nishioka, M. Yamada, D. Kumar, T. Usami, S. Yamada, S. Mizukami, K. Hamaya, Epitaxial growth of CoFe/Ge stacked structures on a perpendicularly magnetized MnGa alloy, Japan. J. Appl. Phys. 64 (2025) 01SP06.
[19] K. Chonan, N.H.D. Khang, M. Tanaka, P.N. Hai, Large magnetoresistance and spin-dependent output voltage in a lateral MnGa/GaAs/MnGa spin-valve device, Japan. J. Appl. Phys. 59 (2020) SGGI08.
[20] M. Ogawa, T. Hara, S. Hasebe, M. Yamanouchi, T. Uemura, Effect of an ultrathin Fe interlayer on the growth of MnGa and spin-orbit-torque induced magnetization switching, Appl. Phys. Express 16 (2023) 063002.
[21] A. Ono, K.Z. Suzuki, R. Ranjbar, A. Sugihara, S. Mizukami, Ultrathin films of polycrystalline MnGa alloy with perpendicular magnetic anisotropy, Appl. Phys. Express 10 (2017) 023005.
[22] T. Suzuki, T. Sasaki, T. Oikawa, M. Shiraishi, Y. Suzuki, K. Noguchi, Room-temperature electron spin transport in a highly doped Si channel, Appl. Phys. Express 4 (2011) 023003.
[23] M. Yamada, M. Tsukahara, Y. Fujita, T. Naito, S. Yamada, K. Sawano, K. Hamaya, Room-temperature spin transport in n-Ge probed by four-terminal nonlocal measurements, Appl. Phys. Express 10 (2017) 093001.
[24] M. Tsukahara, M. Yamada, T. Naito, S. Yamada, K. Sawano, V.K. Lazarov, K. Hamaya, Room-temperature local magnetoresistance effect in n-Ge devices with low-resistive Schottky-tunnel contacts, Appl. Phys. Express 12 (2019) 033002.
[25] K. Hamaya, Y. Fujita, M. Yamada, M. Kawano, S. Yamada, K. Sawano, Spin transport and relaxation in germanium, J. Phys. D: Appl. Phys. 51 (2018) 393001.
[26] H. Kurt, K. Rode, M. Venkatesan, P. Stamenov, J.M.D. Coey, Mn_{3-x}Ga ($0 \leq x \leq 1$): Multifunctional thin film materials for spintronics and magnetic recording, Phys. Status. Solidi B 248 (2011) 2338.
[27] S. Mizukami, T. Kubota, F. Wu, X. Zhang, T. Miyazaki, H. Naganuma, M. Oogane, A. Sakuma, Y. Ando, Composition dependence of magnetic properties in perpendicularly magnetized epitaxial thin films of Mn-Ga alloys, Phys. Rev. B 85 (2012) 014416.
[28] L.J. Zhu, D. Pan, S.H. Nie, J. Lu, J.H. Zhao, Tailoring magnetism of multifunctional Mn_xGa films with giant perpendicular anisotropy, Appl. Phys. Lett. 102 (2013) 132403.
[29] F. Greullet, C. Tiusan, F. Montaigne, M. Hehn, D. Halley, O. Bengone, M. Bowen, W. Weber, Evidence of a symmetry-dependent metallic barrier in fully epitaxial MgO based magnetic tunnel junctions, Phys. Rev. Lett. 99 (2007) 187202.
[30] Y. Takahashi, H. Makuta, T. Shima, M. Doi, Fabrication and magnetic properties of $L1_0$-MnGa highly oriented thin films, T. Magn. Jpn. 1 (2017) 30–33.

[31] T. Kubota, M. Araidai, S. Mizukami, X. Zhang, Q. Ma, H. Naganuma, M. Oogane, Y. Ando, M. Tsukada, T. Miyazaki, Composition dependence of magnetoresistance effect and its annealing endurance in tunnel junctions having Mn-Ga electrode with high perpendicular magnetic anisotropy, Appl. Phys. Lett. 99 (2011) 192509.

[32] B. Achinuq, Y. Fujita, M. Yamada, S. Yamada, A.M. Sanchez, P.J. Hasnip, A. Ghasemi, D. Kepaptsoglou, G. Bell, K. Sawano, K. Hamaya, V.K. Lazarov, Correlation between spin transport signal and Heusler/semiconductor interface quality in lateral spin-valve devices, Phys. Rev. B 98 (2018) 115304.

[33] Z. Nedelkoski, B. Kuerbanjiang, S.E. Glover, A.M. Sanchez, D. Kepaptsoglou, A. Ghasemi, C.W. Burrows, S. Yamada, K. Hamaya, Q.M. Ramasse, P.J. Hasnip, T. Hase, G.R. Bell, A. Hirohata, V.K. Lazarov, Realisation of magnetically and atomically abrupt half-metal/semiconductor interface: $Co_2FeSi_{0.5}Al_{0.5}$/Ge(111), Sci. Rep. 6 (2016) 37282.

[34] K. Kudo, M. Yamada, S. Honda, Y. Wagatsuma, S. Yamada, K. Sawano, K. Hamaya, Room-temperature two-terminal magnetoresistance ratio reaching 0.1% in semiconductor-based lateral devices with $L2_1$-ordered Co_2MnSi, Appl. Phys. Lett. 118 (2021) 162404.

[35] A. Sakuma, Electronic structures and magnetism of CuAu-type MnNi and MnGa, J. Magn. Magn. Mater. 187 (1998) 105–112.

[36] Q.L. Ma, S. Mizukami, T. Kubota, X.M. Zhang, Y. Ando, T. Miyazaki, Abrupt transition from ferromagnetic to antiferromagnetic of interfacial exchange in perpendicularly magnetized $L1_0$-MnGa/FeCo tuned by fermi level position, Phys. Rev. Lett. 112 (2014) 157202.